Aminoglycoside binding to the HIV-1 RNA dimerization initiation site: thermodynamics and effect on the kissing-loop to duplex conversion

Serena Bernacchi[1], Séverine Freisz[1], Clarisse Maechling[2], Bernard Spiess[2], Roland Marquet[1], Philippe Dumas[1] and Eric Ennifar[1],*

[1]Architecture et Réactivité des ARN, UPR 9002 CNRS, Université Louis Pasteur, Institut de Biologie Moléculaire et Cellulaire, 15 rue René Descartes, 67084 Strasbourg and [2]Laboratoire de Pharmacochimie de la Communication Cellulaire, UMR 7081 CNRS/Université Louis Pasteur, Faculté de Pharmacie, 74 route du Rhin, 67401 Illkirch, France

ABSTRACT

Owing to a striking, and most likely fortuitous, structural and sequence similarity with the bacterial 16 S ribosomal A site, the RNA kissing-loop complex formed by the HIV-1 genomic RNA dimerization initiation site (DIS) specifically binds 4,5-disubstituted 2-deoxystreptamine (2-DOS) aminoglycoside antibiotics. We used chemical probing, molecular modeling, isothermal titration calorimetry (ITC) and UV melting to investigate aminoglycoside binding to the DIS loop–loop complex. We showed that apramycin, an aminoglycoside containing a bicyclic moiety, also binds the DIS, but in a different way than 4,5-disubstituted 2-DOS aminoglycosides. The determination of thermodynamic parameters for various aminoglycosides revealed the role of the different rings in the drug–RNA interaction. Surprisingly, we found that the affinity of lividomycin and neomycin for the DIS ($K_d \sim 30\,\text{nM}$) is significantly higher than that obtained in the same experimental conditions for their natural target, the bacterial A site ($K_d \sim 1.6\,\mu\text{M}$). In good agreement with their respective affinity, aminoglycoside increase the melting temperature of the loop–loop interaction and also block the conversion from kissing-loop complex to extended duplex. Taken together, our data might be useful for selecting new molecules with improved specificity and affinity toward the HIV-1 DIS RNA.

INTRODUCTION

Up to now, the fight against HIV essentially relied on multitherapies targeting two out of the three viral enzymes: reverse transcriptase (16 inhibitors approved by the US Food and Drug Administration, FDA) and protease (11 inhibitors approved by the FDA). However, the high mutation and recombination rates of HIV, together with its high replication level, easily allows selection of drug-resistant viruses, thus reinforcing the urgent need for targeting new viral molecules, such as the viral integrase or cellular factors required for HIV-1 replication. Because of the increased interest for RNA in the last few years, several studies pointed out that it could also be an interesting target for small drugs (1–3). Some functional sites within HIV-1 genomic RNA have already been proposed as potential candidates, as the Tat-responsive element TAR (4) or the Rev-responsive element RRE (5), both interacting with the aminoglycoside antibiotic neomycin.

The dimerization initiation site (DIS) of the HIV-1 genomic RNA also constitutes a potentially interesting target since this conserved stem–loop located in the 5′-untranslated region is essential for genome dimerization (6,7), facilitates recombination (8,9) and is required for efficient RNA packaging (7,10) and reverse transcription (7,11). The DIS loop is made of nine nucleotides, six of them forming a self-complementary sequence that promotes genome dimerization by forming a loop–loop complex (also called kissing-loop complex) (12–15), stabilized by flanking unpaired purines (16,17) (Figure 1a). It was shown on short RNA fragments that

*To whom correspondence should be addressed. Tel: +33 3 88 41 70 01; Fax: +33 3 88 60 22 18; Email: e.ennifar@ibmc.u-strasbg.fr
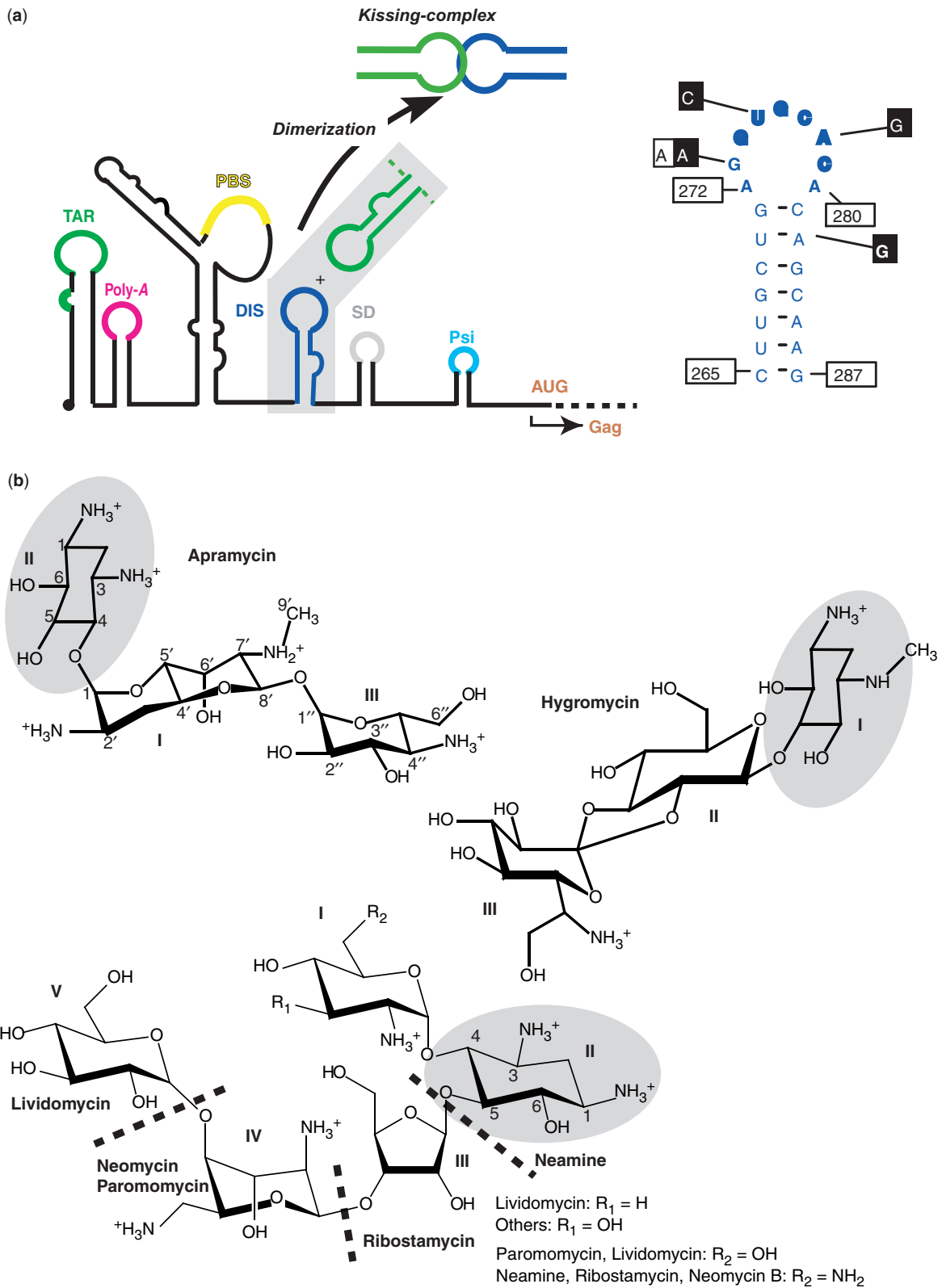
Figure 1. HIV-1 DIS and aminoglycosides. (**a**) Localization of the DIS in the 5′-untranslated region of the HIV-1 genomic RNA, sequence and secondary structure of DIS stem-loops used in this study. The sequence represented here corresponds to HIV-1 subtype A. Sequence variations observed for HIV-1 subtypes B and F are indicated in black and white boxes, respectively. (**b**) Chemical structure of apramycin, hygromycin and of 4,5-disubstituted DOS derivatives used in this study.

this initial kissing-loop complex is further stabilized *in vitro* into an extended duplex form by extension of inter-strand Watson–Crick base pairs (18–20). This conversion is facilitated either by an incubation of the DIS dimer at 55°C, or by the viral nucleocapsid protein NCp7 at 37°C, and might take place during maturation of the viral particle. We have previously solved the crystal structure of the DIS duplex (21) and DIS loop–loop complex (22,23) forms. The kissing-loop complex revealed an unexpected resemblance with the bacterial 16 S ribosomal A site, which is the target of aminoglycoside antibiotics. We showed that, due to structural and sequence similarities, 4,5-disubstituted 2-desoxystreptamine (2-DOS) aminoglycosides, but not 4,6-disubstituted 2-DOS ones, could also specifically bind the DIS kissing-loop with a geometry similar to that observed in the A site (24). In agreement with these early findings, we have recently solved crystal structures of the DIS kissing-loop in complex with several 4,5-disubstituted 2-DOS aminoglycosides and we have shown that the DIS remains accessible to these small drugs within the frame of the complete genome in HIV-1 infected human cells and in viral particles (25,26).

Apramycin and hygromycin B differ in structure from other aminoglycosides (Figure 1b). Apramycin is made of a 4-monosubstituted 2-DOS scaffold containing a bicyclic ring and hygromycin B is made of a 5-monosubstituted 2-DOS with a two ester linkage between rings II and III. Antibacterial activity of these two antibiotics mainly results from blocking ribosome translocation and not by inducing miscoding during translation as for 4,5- and 4,6-disubstituted 2-DOS aminoglycosides (27,28).

Here we showed that apramycin, but not hygromycin, also recognizes the DIS kissing-loop complex; however, its mode of interaction differs from that of 4,5-disubstituted 2-DOS aminoglycosides. Binding free energies of various aminoglycosides to the DIS kissing-loop were obtained by ITC microcalorimetry, revealing a nanomolar affinity for lividomycin and neomycin. These data correlate well with the stabilization of the loop–loop interaction induced by these compounds, as monitored by UV-melting. This stabilization blocks the heat-assisted DIS kissing-loop to extended duplex conversion. These results are in agreement with previous *in vitro* data on much larger viral RNA fragments and *ex vivo* studies and should be valuable for the development of modified aminoglycosides with improved specificity and affinity toward the viral genome.

MATERIALS AND METHODS

Sample preparation

The wild-type 23-mer HIV-1 subtype A DIS RNA, the 23-mer DIS U275C mutant, the 27-mer DIS variant with a stabilized intramolecular stem, and the A site construct, were purchased from Dharmacon (Lafayette, CO, USA). For purification, RNAs were loaded on a Nucleopac PA-100 column (Dionex, Sunnyvale, CA, USA) heated at 70°C and equilibrated in 4 M urea, 20 mM Mes [2-*N*(-Morpholine) ethane sulfonic acid], pH 6.2,

and eluted using a $NaClO_4$ gradient. All aminoglycosides were purchased from Sigma-Aldrich and used without further purification, except neamine, which was obtained from neomycin by acidic treatment as described (29). Kissing-loop complexes were obtained as follows: RNA was diluted to 2 μM [maximum concentration to avoid significant amount of duplex species, see Ref. (30)] in water, heat-denatured at 90°C for 5 min, and then cooled on ice. The A site construct was taken from Ref. (31) and prepared as follows: RNA was diluted to 100 μM in water (to facilitate intermolecular interactions), heated at 90°C for 5 min and cooled to room temperature.

Lead-induced RNA cleavage

Lead(II)-induced cleavage was performed in a buffer containing 2 mM magnesium acetate, 20 mM sodium cacodylate pH 7.0, 25 mM potassium acetate. The 23-mer DIS kissing-loop complex was incubated for 15 min at 25°C in the presence of 5 mM lead(II) acetate. The cleavage reaction was stopped by addition of 19 mM EDTA and by placing the sample in ethanol at −70°C in dry ice. The cleavage was revealed using $5'[\gamma^{32}P]$ATP-labeled RNA as a tracer. Products were analyzed by gel electrophoresis on a denaturing 8 M urea, 20% polyacrylamide gel.

Molecular modeling

The DIS–apramycin model was obtained by superimposing C1 atoms of residues 1405–1409, 1491, 1494 and 1495 in the crystal structure of the apramycin–A site complex (PDB ID 1YRJ) to their DIS counterparts in the crystal structure of the DIS–lividomycin complex (PDB ID 2FD0), resulting in an r.m.s.d. of 0.5 Å on these atoms. Using program O (32), the position of the apramycin was slightly modified (by translation and rotations) to maximize interactions with the DIS RNA. No structural modifications of the RNA were required. Energy minimization of the model was performed with CNS (33).

Isothermal titration calorimetry (ITC)

ITC measurements were performed at 25°C on a MicroCal VP-ITC (MicroCal, Northampton, MA, USA). The buffer contained 25 mM potassium acetate, 2 mM magnesium acetate, 20 mM sodium cacodylate, pH 7.0. Low-salt conditions were chosen at this temperature to avoid conversion of the kissing-loop dimer into the extended duplex form (30). In a typical experiment, 5 μl aliquots of aminoglycoside (100 or 200 μM solution) were injected into a 2 μM DIS kissing-loop complex (1.42 ml sample cell). The duration of each injection was 10 s and the delay between injections was 120 or 240 s. ITC titration curves were analyzed using the software Origin (OriginLab, Northampton, MA, USA). All data obtained with the DIS RNA (excepted with lividomycin) were fitted with a three sequential binding site model (the two specific sites observed in crystal structures, plus one 'average site' aimed at describing all unspecific binding resulting from electrostatic interactions). Data obtained with the DIS and lividomycin, as well as data with the bacterial A site and any antibiotics, were fitted with two independent

Table 1. Binding parameters obtained by ITC measurements for aminoglycoside binding to the HIV-1 subtype A DIS kissing-loop complex and for neomycin with the bacterial ribosomal A site

	K_d (μM)	ΔG (kcal mol^{-1})	ΔH_{int} (kcal mol^{-1})	$T\Delta S$ (kcal mol^{-1})	Number of charges/ contact surface area
Neamine	8.7 (±0.4)	−6.9 (±0.03)	−40.5 (±25)	−33.6 (±25)	4/538 Å^2
Ribostamycin	10.4 (±1.4)	−6.8 (±0.08)	ND	ND	4/565 Å^2
Paromomycin	1.3 (±0.2)	−8.0 (±0.09)	−36.2 (±7)	−29.4 (±7)	4/915 Å^2
Neomycin	0.034 (±0.005)	−10.2 (±0.09)	−9.4 (±2)	0.8 (±2)	6/915 Å^2
Lividomycin	0.032 (±0.007)	−10.2 (±0.13)	−17.5 (±2)	−7.3 (±2)	5/1044 Å^2
Apramycin	5.8 (±1.1)	−7.1 (±0.11)	−51.7 (±11)	−44.6 (±11)	5/–
Tobramycin	14.5 (±0.1)	−6.6 (±0.01)	ND	ND	4/–
Neomycin (A site)	1.55 (±0.07)	−7.9 (±0.03)	−16.2 (±1.0)	−8.3 (±1.0)	6/–

ΔH_{int} was calculated from ΔH_{obs} as described in the Methods section. ND stands for 'not determined', since accurate values of ΔH could not be obtained. The ΔS value for neomycin is null within experimental errors. The number of expected positive charges as well as the drug/RNA contact surface area for known structures are also indicated [taken from Ref. (25)], excepted for paromomycin where the contact surface area was extrapolated for the neomycin/DIS structure.

binding sites, resulting in a significant better fit. Standard free energies of binding and entropic contributions were obtained, respectively, as $\Delta G = -RT \ln(K_a)$ and $T\Delta S = \Delta H - \Delta G$, from the K_a and ΔH values derived from ITC curve fitting. In our experimental conditions, the product $K_a \times [RNA] \times N$, where N is the number of binding sites, lies in the 0.1–1000 range (0.4 for ribostamycin to 125 for lividomycin), allowing an accurate and simultaneous determination of binding parameters by ITC (34). It has been shown by Pilch and coworkers (35) that for aminoglycoside binding to the ribosomal A site, the intrinsic binding enthalpy ΔH_{int} differs from the observed binding enthalpy ΔH_{obs} and can be obtained by the following equation:

$$\Delta H_{obs} = \Delta H_{int} + \Delta H_{ion}\Delta n$$

where ΔH_{ion} represents the heat of ionization from the considered buffer, and Δn the number of protons linked to binding at a specific pH. This correction (a minor one in our case) was applied using the ionization heat (ΔH_{ion}) for cacodylate at 25°C [−0.47 kcal mol^{-1} per proton according to Ref. (36)] and the Δn values determined in Ref. (37) to derive the intrinsic binding enthalpies presented in Table 1.

UV-melting studies

The 27-mer DIS variant sequence with a stabilized intramolecular stem was diluted to 2.5 μM in 500 μl of water, heat-denatured at 90°C for 5 min and chilled at 0°C. After 10 min at this temperature, 55.5 μl of a 10× concentrated buffer (made with 250 mM potassium acetate, 500 μM magnesium acetate and 200 mM sodium cacodylate, pH 7.0) was added. The sample was then placed at 20°C for 10 min and 1 μl of a 6 mM aminoglycoside solution was added to the RNA sample (10.7 μM final antibiotic concentrations). Absorbance versus temperature melting curves were measured at 260 nm with a heating rate of 0.5°C min^{-1} on a UVIKON-XL spectrometer (SECOMAM, Domont, France) equipped with a Peltier thermo-stated cell holder. Each melting experiment in presence of aminoglycoside was performed six times for better statistics. UV-melting curves and their derivatives

were smoothed with a Fourier-based filtering procedure programmed with Mathematica (Wolfram Res., Champaign, IL, USA).

DIS kissing-loop to extended duplex conversion

DIS 23-mer containing a 5-bromouridine on U3 was folded as a kissing-loop at a 12 μM concentration (in RNA stands) in a buffer containing 25 mM potassium acetate and 20 mM sodium cacodylate pH 7.0. For each experiment, 1.2 μl of aminoglycoside at a 1 mM concentration was added to 11.1 μl of RNA sample and incubated 1 h at 20 or 55°C (in an incubator to avoid condensation of water on the Eppendorf tube and sample concentration). Each sample was then loaded in a 15% polyacrylamide gel, either in semi-denaturing conditions (TB 1×, migration at room temperature, 6 W), or in a native conditions (TB 1×, magnesium chloride 1 mM, migration at 4°C, 6 W). The gel was then stained in ethidium bromide for analysis.

RESULTS AND DISCUSSION

Apramycin binding to the DIS kissing-loop complex

Chemical footprinting using lead(II) acetate was used to investigate apramycin and hygromycin B binding to the DIS kissing-loop complex. Using this method, it was previously shown that neomycin, paromomycin and lividomycin completely protect the DIS kissing-loop complex from a specific lead(II)-induced cleavage (24,26). An almost complete protection of the DIS RNA was also observed upon addition of 25 μM of apramycin. The protection was slightly weaker than that observed at the same concentration of paromomycin or neomycin, but similar to the protection observed with lividomycin (Figure 2). This result confirms a recent report indicating that apramycin binds the DIS kissing-loop (38). However, no significant protection was observed with hygromycin (Figure 2), even when using millimolar concentrations of drug (data not shown).

Structural insight into the apramycin/DIS complex was obtained by 3D molecular modeling starting from the X-ray structure of apramycin bound to the
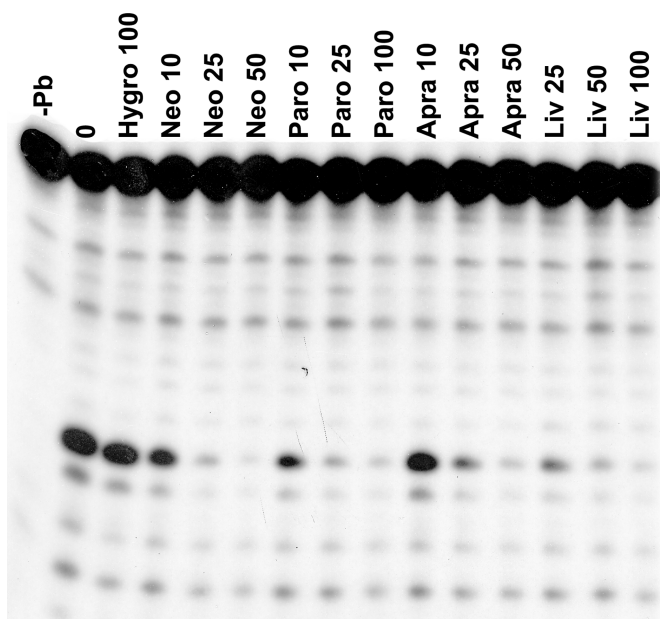
Figure 2. Inhibition of the lead-induced cleavage by aminoglycosides hygromycin, neomycin, paromomycin, apramycin and lividomycin. Numbers correspond to μM concentration of the antibiotic. (-Pb) and (0) correspond to control lanes without aminoglycoside, without and with lead(II) acetate, respectively.

bacterial A site (39). Apramycin was docked into the HIV-1 subtype F DIS kissing-loop complex as observed in the crystal structures with aminoglycosides (26), since docking to unliganded structures of the kissing-loop complex led to a steric clash with the bicyclic moiety of apramycin. The bound structures mainly differ from the unliganded kissing-loop by a shift from a C2′-*endo* to a C3′-*endo* conformation of G271 upon drug binding. The model revealed a different binding pattern of apramycin as compared to 4,5-disubstituted 2-DOS aminoglycosides (Figure 3a). First, the latter interact with the loop–loop helix and the major groove of both stems, whereas apramycin interacts also with the loop–loop helix but with the minor groove of both stems (Figure 3a). Second, according to the model, apramycin probably enters the kissing-loop through the minor groove of the RNA whereas, according to the X-ray structures, 4,5-disubstituted 2-DOS aminoglycosides most likely enter through the major groove (Figure 3a).

According to the model, the 2-DOS ring occupies the same position in the apramycin/DIS and 4,5-disubstituted 2-DOS aminoglycosides/DIS complexes (Figure S1). It interacts simultaneously with both RNA strands in the loop–loop helix (Figure 3b and c) and achieves a sequence-specific recognition of the RNA through interactions with the bases of A278, C279, G274′, U275′ and G276′ (the prime stands for the second RNA strand) (Figure S2). Since U275 and A278 are involved into apramycin recognition, we can anticipate that, as already observed for other aminoglycosides (24,26), apramycin binding to the DIS will be restricted to HIV-1 subtypes with a 5′**GU**275**GCA**278**C**3′ DIS self-complementary sequence in the loop, therefore excluding HIV-1 subtype

B DIS with a 5′**GC**275**GCG**278**C**3′ sequence. Similarly to ring I of the neamine class aminoglycoside, the bicyclic moiety of apramycin is involved in a pseudo Watson–Crick base pair with the unpaired A280 (Figure 3b and c), thus preventing any flipped-in conformation of purines 272 and 273. Because of the protrusion of its ring III in the minor groove close to bulged-out purines 272 and 273 (Figure 3a and b), apramycin might indirectly interact with these bases through water molecules or ions and influence their *syn/anti* conformation: such a conformational flexibility was observed in crystal structures of subtype A DIS kissing-loop complexes (22,23). Finally, ring III of apramycin interacts with the sugar-phosphate backbone of A282 and G271, as well as with the sugar edge of G271 (Figure 3b and c). In addition to 12 possible direct drug/RNA interactions suggested by the model, several water- or ion-mediated interactions likely reinforce the binding, as observed for neamine-class aminoglycosides (26), but these cannot be reasonably predicted by a model.

The crystal structure of a bacterial 30 S ribosomal subunit (containing the A site) bound to hygromycin (40) was also used to build a DIS/hygromycin model (data not shown) in order to understand the lack of binding. It appears that, unlike apramycin and 4,5-disubstituted 2-DOS aminoglycosides, hygromycin would require an inversion of the C269–G283 base pair into G269–C283, as observed in the bacterial ribosomal A site. This difference with the A-site precludes hygromycin binding to the DIS dimer.

Determination of the thermodynamic parameters of aminoglycoside/DIS binding and comparison with the A site

Isothermal titration calorimetry (ITC) was used to characterize aminoglycoside binding to the DIS kissing-loop complex. Unlike other techniques such as chemical footprinting or fluorescence spectroscopy that are indirect methods, ITC directly provides a full thermodynamic profile of the drug/RNA interaction (34) and does not require any modification of the RNA for labeling. In addition, this method was already successfully employed to characterize aminoglycoside/A site interactions (35,37,41–43). We investigated the binding to the HIV-1 subtype-A DIS of neamine, ribostamycin, paromomycin, neomycin, lividomycin, apramycin and tobramycin. Experimental conditions were chosen to be compatible with the DIS kissing-loop complex and to avoid any interference with the spontaneous conversion into the extended duplex form of the DIS in the timescale of the experiment (30): RNA concentration did not exceed 2 μM in a low-salt buffer, and the temperature was set to 25°C. Great care was taken to estimate the unspecific binding of the positively charged aminoglycoside antibiotics on the RNA. For that goal, we monitored their binding to a standard A-form RNA helix of 22 bp with a sequence very similar to that of the DIS, but deprived of unpaired residues and base-pair mismatches and thus of specific binding sites (Figure S3). Unspecific interactions were also investigated with a DIS hairpin monomer using a DIS U275C mutant that cannot form a kissing-loop
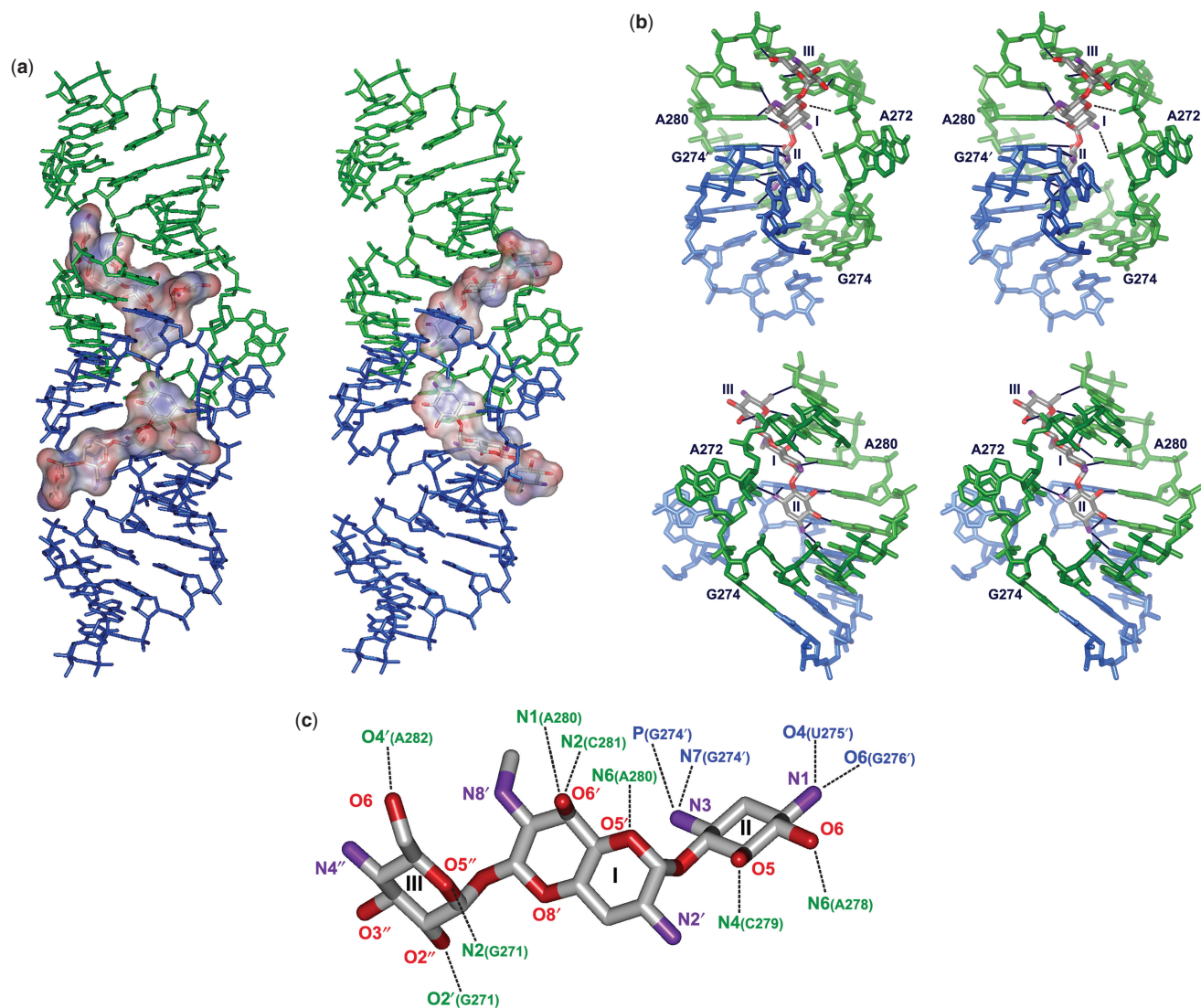
Figure 3. (a) Representation of the solvent accessibility surface of aminoglycosides (probe radius 1.4 Å) in the DIS/lividomycin crystal structure (left) and the DIS/apramycin model (right) with the same orientation of the RNA kissing-loop complex. These views clearly depict the different binding geometry of these two aminoglycosides. (b) Two different stereoviews of the apramycin–DIS complex showing direct RNA–drug interactions (black lines). Dotted lines on the top view indicate probable water-mediated drug–RNA interaction. (c) Expected apramycin–RNA direct interactions deduced from the model.

dimer, as well as with a HIV-1 subtype-B DIS sequence that is not recognized by aminoglycosides (24). The 4,6-disubstituted 2-DOS tobramycin that does not bind the DIS kissing-loop (24) was also used to determine aminoglycoside unspecific binding to the wild-type subtype A DIS kissing-loop complex. As expected, all these situations were characterized by a weak exothermic signal (Figure 4a) and led essentially to superimposable titration curves (Figure S3). They can therefore be considered as typical titration curves for unspecific aminoglycoside/RNA interactions.

As observed for the A site, specific aminoglycoside binding to the DIS is followed by exothermic heat bursts due to protonation of several amino groups (37). It has been shown that aminoglycoside binding to the A site is strongly dependent on the pH and on

drug protonation: at low pH, already protonated aminoglycosides bind with a higher affinity to the A site than at high pH, resulting in lower exothermic signal and a reduced enthalpic contribution (35,37). We conducted our ITC experiments at pH 7.0 to take benefit of a rather large calorimetric signal and to obtain binding parameters at physiological pH. Figure 4 shows representative ITC profiles for specific binding resulting from the injection of neamine (b) and lividomycin (c) in a solution of subtype-A DIS kissing-loop complex at pH 7.0. No assumption was made about the cooperativity of the two binding sites within a kissing-loop complex. Based on crystal structures, some anti-cooperativity was possible because of the close proximity of the two positively charged N1 positions of the 2-DOS ring (~4.4 Å). Fitting of titration curves, however, yielded almost identical equilibrium constants
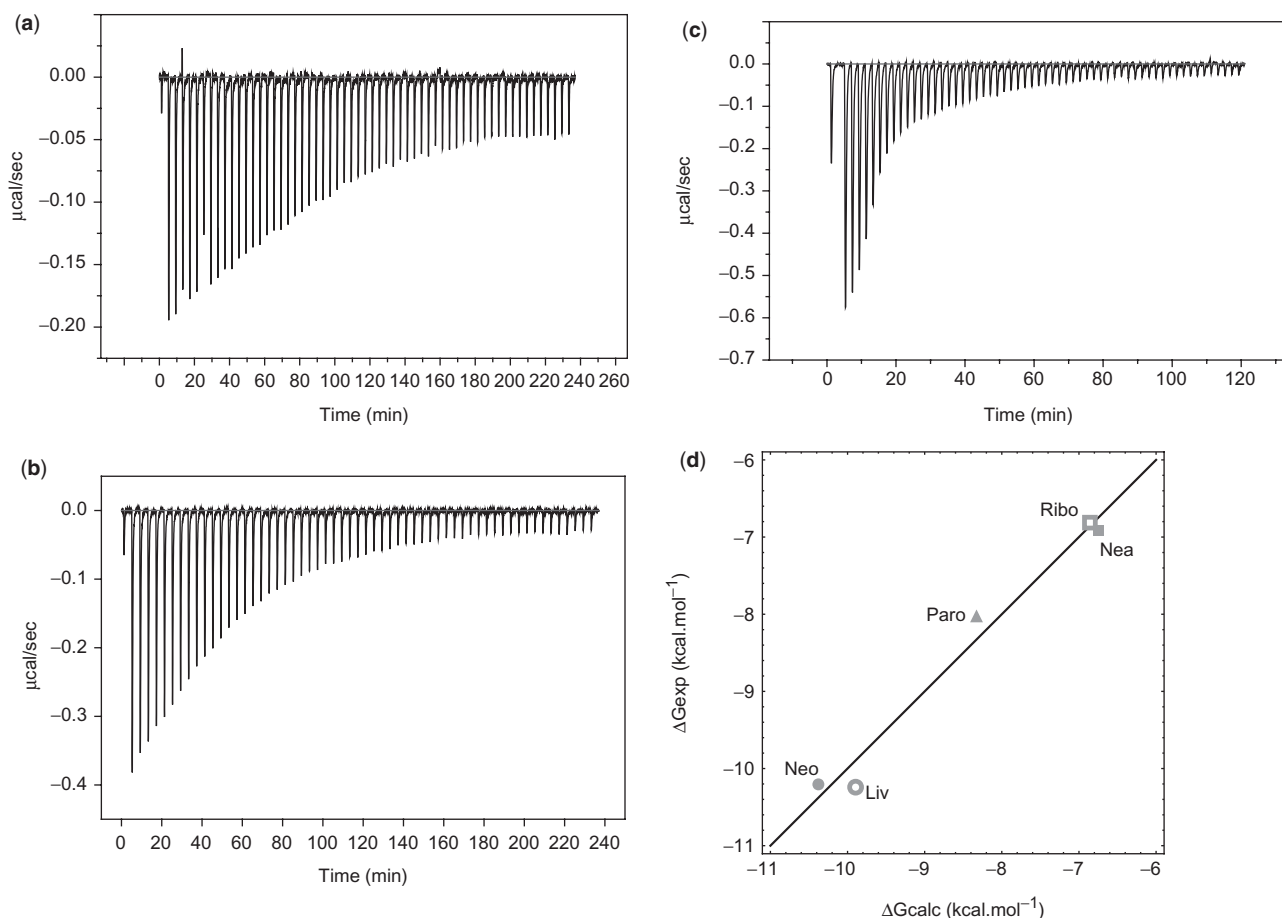
Figure 4. ITC profiles for the titration of (**a**) lividomycin on the monomeric DIS U275C mutant, which is typical of unspecific binding, (**b**) of neamine and (**c**) of lividomycin on the subtype A DIS kissing-loop, which are typical of weak and strong specific binding, respectively. Each heat burst curve is the result of a 5 µl injection of 200 µM drug in a 2 µM RNA solution (1.42 sample cell). (**d**) Comparison of the measured free energy (△Gexp) and the calculated free energy (△Gcalc) based on charge number and drug/RNA contact surface area observed in crystal structures. Since no crystal structure of the paromomycin/DIS complex was obtained, surface area for paromomycin was considered to be identical to the neomycin one (similar contacts are expected).

(after correction for the expected statistical factor one-fourth between two successive binding sites), leading to the conclusion that they can be considered as independent and equivalent.

In agreement with our previous chemical probing data (26), lividomycin and neomycin were the strongest binders with sub-micromolar affinities (Table 1), followed by paromomycin. It was shown that only these three drugs are able to efficiently protect the DIS of large HIV-1 RNA fragments toward chemical probes (26). The affinity drops to ~10 µM for neamine and ribostamycin, which were inefficient in footprinting experiments. This confirms that, as anticipated from our previous studies, rings IV and V are extremely important for aminoglycoside affinity, although they interact only unspecifically with the RNA sugar-phosphate backbone. By contrast, rings I, II and III provide all structure- and sequence-specific contacts. Interestingly, as already observed for the bacterial A site (44), the affinity of neamine is higher than that of ribostamycin despite the larger number of drug–RNA interactions in the DIS/ribostamycin complex. An inter-mediate K_d value was obtained for apramycin (5.8 µM),

which protects the 23-nt DIS significantly better than neamine against lead-induced cleavage. Finally, only unspecific binding was observed with tobramycin (~14 µM), in agreement with the previous results (24). It is nevertheless obvious that unspecific binding is variable and depends on the number of positive charges of each antibiotic molecule. Affinities determined by ITC are roughly consistent with values obtained by fluorescence techniques (38). Differences might be due to perturbations of the conformation of purines 272 and 273 when they are substituted by 2-aminopurines (2AP) for fluorescence labeling. Indeed, it has been shown for the A site that substitution of unpaired adenines by 2-AP affects the bulged-in/-out equilibrium (45) and that A-2AP base pairs are more stable than A–A interactions (Figure S4).

The observed standard free energies (ΔG_{exp}) were then compared to drug/RNA interacting surface area deduced from X-ray structures (25), and to the number of positive charges. For that goal, calculated free energies (ΔG_{calc}) were estimated according to the simple linear model:

$$\Delta G_{calc} = \alpha N + \beta S$$

where N is the number of positive charges of the drug, and S is the drug/RNA contact surface area. Linear regression yielded $\alpha = -1.1$ (± 0.15) kcal mol^{-1} per positive charge and $\beta = -1.0$ kcal mol^{-1} for 240 (± 45) Å^2. As simple as it may be, this model yields a rather good correlation between observed and calculated ΔG (Figure 4d). However, such numerical values are DIS-specific, particularly for the term α, which should be strongly structure-dependent. In the present situation, the fraction of free energy due to the charges is $65 \pm 1.5\%$ for neamine, ribostamycin and neomycin and $54 \pm 1\%$ for paromomycin and lividomycin (Table 1). These values are expected to change in different ionic-strength conditions.

Interestingly, it is possible to perform the same calculations for neamine, ribostamycin, paromomycin and neomycin by considering the experimental data on the A site from Ref. (46). The fit (with the number of positive charges listed in Table 1) is also very good with $\alpha = -0.72$ (± 0.18) kcal mol^{-1} per positive charge and $\beta = -1.0$ kcal mol^{-1} for 150 (± 24) Å^2. In this case, the fraction of free energy due to the charges is $41.5 \pm 1.5\%$ for neamine, ribostamycin and neomycin and 31% for paromomycin. The salt conditions in Ref. (46) were 150 mM NaCl, 10 mM HEPES, pH 7.4 in comparison of 25 mM potassium acetate, 2 mM magnesium acetate, 20 mM Na cacodylate, pH 7.0 in our study. Notably, the agreement with experimental data obtained with our simple ΔG modeling is at least as good as the one obtained in Ref. (47) with a much more elaborate method involving the Poisson–Boltzmann equation.

In order to obtain an accurate comparison of aminoglycoside binding to the HIV-1 DIS and to the ribosomal A site, we performed an ITC experiment with neomycin in the same experimental conditions than with the DIS, but on a minimal 'double A site' RNA duplex. The latter has already been used for crystallization and structure solution of the bacterial A site with aminoglycosides (31). The two A-site motifs are separated by a 6-bp helical part (~ 17 Å) and can therefore be considered as independent binding sites. This construct was chosen because it is as close as possible to the DIS kissing-loop: both RNA have two antibiotics binding sites and are of same size (similar unspecific binding is therefore expected). In these quite comparable conditions, a K_d of 1.55 µM was found for neomycin (Table 1 and Figure S5). Rather surprisingly, neomycin thus binds the DIS kissing-loop complex with a 40-fold higher affinity than its natural target, the bacterial ribosomal A site. In the light of the aminoglycoside/DIS crystal structure, this enhanced affinity is well explained by additional structure-specific interactions between ring I and the phosphates of the DIS RNA. These direct or cation-mediated interactions are specific to the kissing-loop topology and cannot be observed in equivalent aminoglycoside/A site complexes (25,26).

Stabilization of the DIS loop–loop interaction upon drug binding

We then analyzed the impact of aminoglycoside binding on the DIS loop–loop helix stability using UV-melting. To avoid problems in melting curves interpretation [because of overlapping signals of the 7 bp stem, the 6 bp loop–loop helix, and hairpin to duplex conversion (30)], a 27-nt DIS variant sequence was used to make possible the distinction between the kissing-loop dissociation and the stem melting: the stem of this DIS mutant was stabilized by the substitution of two G-C for two A-U base pairs (not involved into drug binding) and the addition of two terminal G-C base pairs (Figure 5). This stabilization shifted the melting of the stem toward higher temperatures without affecting the melting temperature of the loop–loop helix. Control UV-melting experiments were first conducted in absence of ligand and with increasing concentrations of RNA. The transition observed is concentration-dependent, shifting from 38.5 to 44°C when the RNA concentration increased from 1.15 to 3.1 µM, in agreement with the bimolecular dissociation of the loop–loop helix. From a van't Hoff analysis (48) we derived an enthalpy of loop–loop interaction $\Delta H = -34$ kcal mol^{-1} (Figure 5). Addition of aminoglycosides induced a displacement of the loop–loop melting to higher temperatures. The shift (ΔT_m) ranged from 7.5°C upon addition of ribostamycin, to 24.8°C upon addition of neomycin (Table 2 and Figure S6). The stabilization is roughly consistent with affinities determined previously: a drug with a low K_d induces a strong stabilization of the kissing-loop complex. A negative control was also performed with hygromycin, which did not significantly stabilize the kissing-loop complex ($\Delta T_m = 0.3°C$). Thus, aminoglycosides can be separated into two clusters: ribostamycin, neamine and apramycin (with K_d values in the 5–12 µM range) stabilize poorly the kissing-loop interaction (less than 14°C), whereas paromomycin, neomycin and lividomycin having much lower K_d values (1.3 µM, 34 and 32 nM, respectively) stabilize it by more than 20°C. These results correlate very well with previous biochemical experiments performed on much larger RNA fragments encompassing the complete 5′-untranslated region of the viral genome (26). It was found that neomycin, lividomycin and paromomycin strongly increased the lifetime of the DIS kissing-loop complex, whereas no significant effect was observed in presence of neamine and ribostamycin. We can therefore postulate that beyond a certain value of the ΔT_m, comprised between 9.1°C (for neamine) and 19.5°C (for lividomycin), aminoglycoside binding stabilize the DIS kissing-loop in the context of large viral RNA fragments *in vitro*.

These results also suggest that UV-melting is a simple and convenient way to monitor aminoglycoside binding to the DIS kissing-loop complex: using a multicell holder, it is possible to automatically screen several drugs at the same time and to derive information about affinity and stabilization of these molecules.

Aminoglycoside binding inhibits the DIS kissing-loop to extended duplex transition

The impact of aminoglycoside binding on the DIS kissing-loop complex to extended duplex conversion was evaluated using biochemical techniques. It was shown that this NCp7-assisted conversion can also be facilitated by incubating the DIS at 55°C, without NCp7 (49,50),
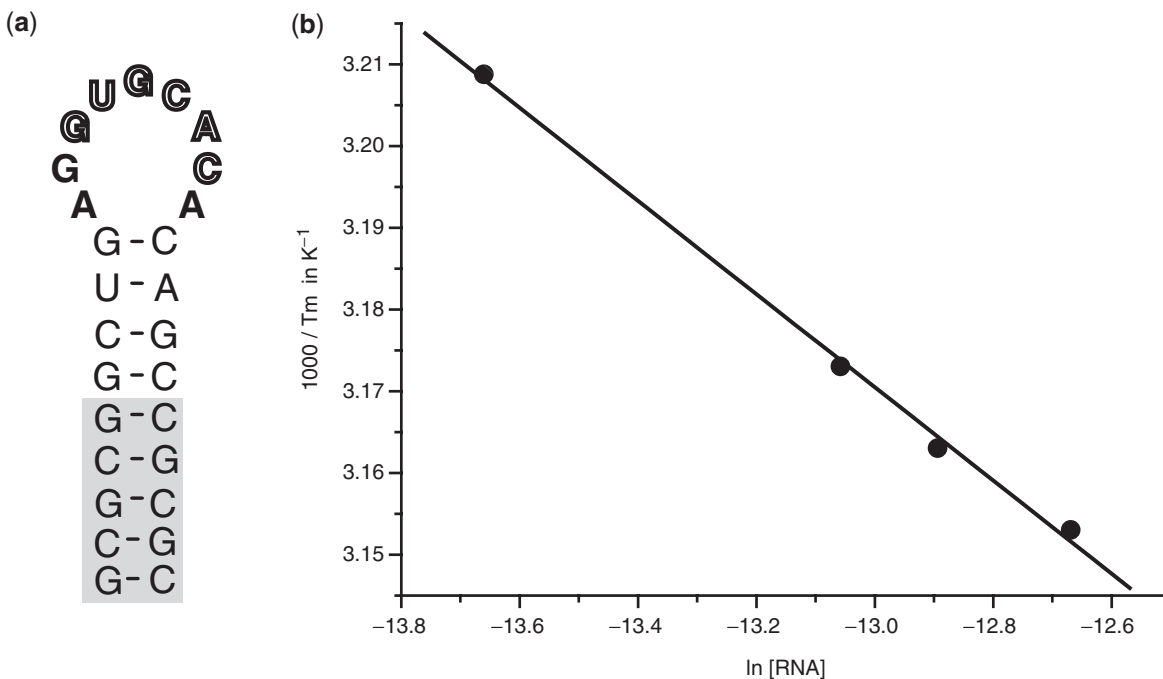
Figure 5. (a) 27-mer RNA sequence used for UV-melting studies. Mutations introduced to stabilize the DIS stem are boxed in gray. The self-complementary sequence is bolded. (b) van't Hoff analysis of the concentration-dependent melting curve for the DIS kissing-loop interaction in absence of drug.

Table 2. Melting temperatures observed for the DIS kissing-loop complex alone (for an RNA concentration of 2.5 μM) and in presence of various aminoglycoside antibiotics at 10.7 μM final concentration

	T_m (°C)	ΔT_m (°C)
RNA only	43.0 (±1.4)	–
Neamine	52.1 (±2.3)	9.1
Ribostamycin	50.5 (±2.6)	7.5
Paromomycin	63.4 (±0.9)	20.4
Neomycin	67.8 (±1.1)	24.8
Lividomycin	62.5 (±0.4)	19.5
Apramycin	56.9 (±0.7)	13.9
Hygromycin	43.3 (±4.3)	0.3

Figure 6. Semi-denaturing gel obtained after 1 h of incubation of DIS kissing-loop at 55°C (or 20°C) in presence of 100 μM hygromycin, lividomycin, neomycin, paromomycin, apramycin, ribostamycin and neamine. The lower band corresponds to DIS hairpin resulting from kissing-loop complex dissociation in semi-denaturing conditions, whereas the top band corresponds to DIS duplex. The 'C275' lane is a DIS U275C mutant that cannot form a kissing-loop complex and is poorly converted into duplex. The '0' lane corresponds to the addition of water instead of drug.

resulting in duplex dimers of similar conformations (51). The distinction between the DIS kissing-loop and extended duplex dimers can be performed by gel electrophoresis in semi-denaturing conditions: in absence of magnesium and at room temperature, the loop–loop interaction is unstable, resulting in DIS hairpin monomers, whereas duplex dimers are resistant to such experimental conditions (20,52). A control DIS monomer is obtained using the DIS C275 mutant, where the U275C mutation in the self-complementary sequence prevents formation of a kissing-loop dimer and strongly disfavors the formation of the duplex dimer (30).

After 1 h of incubation at 55°C, a majority of DIS was converted into duplex in absence of drug (Figure 6, lane '0' at 55°C), whereas only trace amount of duplex was visible after 1 h at 20°C (Figure 6, lane '0' at 20°C) or at 37°C (data not shown). Addition of various aminoglycoside antibiotics (100 μM final concentration)
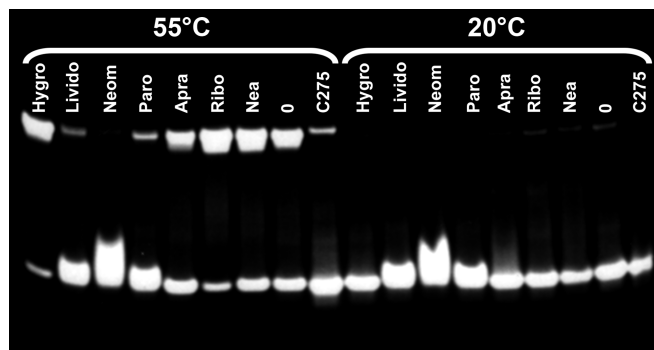
differently affects this conversion (Figure 6). Hygromycin (used here as a negative control) strongly favors the duplex formation at 55°C and the amount of duplex also increased with ribostamycin, but was not significantly affected by apramycin or neamine. The most pronounced and interesting effect was observed with the three drugs having the strongest stabilization effect on the kissing-loop according to UV-melting studies: lividomycin, neomycin and paromomycin strongly inhibit the conversion into duplex (Figure 6). In particular, no trace of duplex dimer

could be observed with neomycin, which is also the best DIS kissing-loop complex binder.

To check that the observed monomer in semi-denaturing conditions really results from kissing-loop dissociation, and not from an inhibition of the loop–loop interaction, an aliquot of the RNA incubated at $55°C$ in presence of aminoglycosides was loaded on a gel in native conditions at $4°C$ in presence of magnesium. This experiment confirmed that lividomycin, neomycin and paromomycin do not prevent the kissing-loop interaction at $55°C$ (Figure S7), but indeed block the kissing-loop to dimer conversion. Experiments performed with increasing aminoglycoside concentration show an IC_{50} for neomycin, lividomycin and paromomycin of $\sim 500\,\mu M$ at $55°C$ (Figure S8 and data not shown). Inhibition of the conversion could also be observed with apramycin at higher level of drug concentration ($>1\,mM$, data not shown).

CONCLUSIONS

Here we show that apramycin, but not hygromycin, binds the DIS kissing-loop complex. Based on molecular modeling, the apramycin/DIS interaction is expected to differ from the interaction between the DIS and the 4,5-disubstituted 2-DOS aminoglycosides. In particular, the minor groove of the DIS stem might be involved into apramycin recognition in addition to the loop–loop interstrand helix, thus suggesting new potential drug/RNA interactions for rational drug design. Binding parameters of several aminoglycosides were determined by ITC microcalorimetry, showing a sub-micromolar affinity of the DIS kissing-loop complex for neomycin and lividomycin, and low micromolar affinity for paromomycin and apramycin. On the contrary, no specific binding was detected for hygromycin and for the 4,6-disubstituted 2-DOS tobramycin.

Binding of paromomycin, lividomycin and neomycin results in a strong stabilization of the DIS loop–loop interaction that was monitored by UV melting. This stabilization traps the kissing-loop complex, blocking its heat-assisted conversion into the extended duplex form of the DIS. We are now investigating possible effects of this stabilization on various steps of the viral replication. First, viral reverse transcription might be affected at the late stage of the $(-)$ strand DNA synthesis, since stabilization of the kissing-loop complex could induce pauses of the viral reverse transcriptase and its dissociation from the reverse transcription complex. Second, the effect of aminoglycosides on the NCp7 chaperone activity has to be evaluated. This positively charged small protein covering the viral genome did not obstruct aminoglycoside access to the DIS in viral particles or infected cells (26), but might indeed hinder the aminoglycoside effect *in vivo* through its efficient nucleic acids chaperone activity. Consequently, we are currently analyzing the effect of aminoglycosides on the NCp7-assisted isomerization of the kissing-loop complex in the extended duplex.

Finally, it was shown that DIS kissing-loop interactions can be used as a building block for nucleic acid-based nanostructures with linear or circular interactions (53–55). We suggest that aminoglycoside antibiotics might be used as a 'specific glue' to enhance the stability of such nanostructures based on DIS kissing-loop motifs. The possibility of varying the stability of particular interactions would open the way of making transient bonds, which should permit building up more complicate structures.

REFERENCES

1. Hermann,T. (2005) Drugs targeting the ribosome. *Curr. Opin. Struct. Biol.*, **15**, 355–366.
2. Tor,Y. (2003) Targeting RNA with small molecules. *Chembiochem*, **4**, 998–1007.
3. Vicens,Q. and Westhof,E. (2003) RNA as a drug target: the case of aminoglycosides. *Chembiochem*, **4**, 1018–1023.
4. Wang,S., Huber,P.W., Cui,M., Czarnik,A.W. and Mei,H.Y. (1998) Binding of neomycin to the TAR element of HIV-1 RNA induces dissociation of Tat protein by an allosteric mechanism. *Biochemistry*, **37**, 5549–5557.
5. Zapp,M.L., Stern,S. and Green,M.R. (1993) Small molecules that selectively block RNA binding of HIV-1 Rev protein inhibit Rev function and viral production. *Cell*, **74**, 969–978.
6. Haddrick,M., Lear,A.L., Cann,A.J. and Heaphy,S. (1996) Evidence that a kissing loop structure facilitates genomic RNA dimerisation in HIV-1. *J. Mol. Biol.*, **259**, 58–68.
7. Paillart,J.-C., Berthoux,L., Ottmann,M., Darlix,J.-L., Marquet,R., Ehresmann,C. and Ehresmann,B. (1996) A dual role of the dimerization initiation site of HIV-1 in genomic RNA packaging and proviral DNA synthesis. *J. Virol.*, **70**, 8348–8354.
8. Balakrishnan,M., Fay,P.J. and Bambara,R.A. (2001) The kissing hairpin sequence promotes recombination within the HIV-I 5′ leader region. *J. Biol. Chem.*, **276**, 36482–36492.
9. Chin,M.P., Rhodes,T.D., Chen,J., Fu,W. and Hu,W.S. (2005) Identification of a major restriction in HIV-1 intersubtype recombination. *Proc. Natl Acad. Sci. USA*, **102**, 9002–9007.
10. Berkhout,B. and van Wamel,J.L. (1996) Role of the DIS hairpin in replication of human immunodeficiency virus type 1. *J. Virol.*, **70**, 6723–6732.
11. Shen,N., Jette,L., Liang,C., Wainberg,M.A. and Laughrea,M. (2000) Impact of human immunodeficiency virus type 1 RNA dimerization on viral infectivity and of stem-loop B on RNA dimerization and reverse transcription and dissociation of dimerization from packaging. *J. Virol.*, **74**, 5729–5735.
12. Laughrea,M. and Jetté,L. (1994) A 19-nucleotide sequence upstream of the 5′ major splice donor site is part of the dimerization domain of human immunodeficiency virus 1 genomic RNA. *Biochemistry*, **33**, 13464–13474.

13. Muriaux,D., Girard,P.M., Bonnet-Mathonière,B. and Paoletti,J. (1995) Dimerization of HIV-1Lai RNA at low ionic strength. *J. Biol. Chem.*, **270**, 8209–8216.

14. Paillart,J.C., Skripkin,E., Ehresmann,B., Ehresmann,C. and Marquet,R. (1996) A loop-loop kissing complex is the essential part of the dimer linkage of genomic HIV-1 RNA. *Proc. Natl Acad. Sci. USA*, **93**, 5572–5577.

15. Skripkin,E., Paillart,J.C., Marquet,R., Ehresmann,B. and Ehresmann,C. (1994) Identification of the primary site of the human immunodeficiency virus type 1 RNA dimerization *in vitro*. *Proc. Natl Acad. Sci. USA*, **91**, 4945–4949.

16. Clever,J.L., Wong,M.L. and Parslow,T.G. (1996) Requirements for kissing-loop-mediated dimerization of human immunodeficiency virus RNA. *J. Virol.*, **70**, 5902–5908.

17. Paillart,J.C., Westhof,E., Ehresmann,C., Ehresmann,B. and Marquet,R. (1997) Non-canonical interactions in a kissing loop complex: the dimerization initiation site of HIV-1 genomic RNA. *J. Mol. Biol.*, **270**, 36–49.

18. Muriaux,D., Rocquigny,H.D., Roques,B.P. and Paoletti,J. (1996) NCP7 activates HIV-1 Lai RNA dimerization by converting a transient loop-loop complex into a stable dimer. *J. Biol. Chem.*, **271**, 33686–33692.

19. Rist,M.J. and Marino,J.P. (2002) Mechanism of nucleocapsid protein catalyzed structural isomerization of the dimerization initiation site of HIV-1. *Biochemistry*, **41**, 14762–14770.

20. Takahashi,K.I., Baba,S., Chattopadhyay,P., Koyanagi,Y., Yamamoto,N., Takaku,H. and Kawai,G. (2000) Structural requirement for the two-step dimerization of human immunodeficiency virus type 1 genome. *RNA*, **6**, 96–102.

21. Ennifar,E., Yusupov,M., Walter,P., Marquet,R., Ehresmann,B., Ehresmann,C. and Dumas,P. (1999) The crystal structure of the dimerization initiation site of genomic HIV-1 RNA reveals an extended duplex with two adenine bulges. *Structure*, **7**, 1439–1449.

22. Ennifar,E. and Dumas,P. (2006) Polymorphism of bulged-out residues in HIV-1 RNA DIS kissing complex and structure comparison with solution studies. *J. Mol. Biol.*, **356**, 771–782.

23. Ennifar,E., Walter,P., Ehresmann,B., Ehresmann,C. and Dumas,P. (2001) Crystal structures of coaxially stacked kissing complexes of the HIV-1 RNA dimerization initiation site. *Nat. Struct. Biol.*, **8**, 1064–1068.

24. Ennifar,E., Paillart,J.C., Marquet,R., Ehresmann,B., Ehresmann,C., Dumas,P. and Walter,P. (2003) HIV-1 RNA dimerization initiation site is structurally similar to the ribosomal A site and binds aminoglycoside antibiotics. *J. Biol. Chem.*, **278**, 2723–2730.

25. Ennifar,E., Paillart,J.C., Bernacchi,S., Walter,P., Pale,P., Decout,J.L., Marquet,R. and Dumas,P. (2007) A structure-based approach for targeting the HIV-1 genomic RNA dimerization initiation site. *Biochimie*, **89**, 1169–1290.

26. Ennifar,E., Paillart,J.C., Bodlenner,A., Walter,P., Weibel,J.M., Aubertin,A.M., Pale,P., Dumas,P. and Marquet,R. (2006) Targeting the dimerization initiation site of HIV-1 RNA with aminoglycosides: from crystal to cell. *Nucleic Acids Res.*, **34**, 2328–2339.

27. Gonzalez,A., Jimenez,A., Vazquez,D., Davies,J.E. and Schindler,D. (1978) Studies on the mode of action of hygromycin B, an inhibitor of translocation in eukaryotes. *Biochim. Biophys. Acta*, **521**, 459–469.

28. Perzynski,S., Cannon,M., Cundliffe,E., Chahwala,S.B. and Davies,J. (1979) Effects of apramycin, a novel aminoglycoside antibiotic on bacterial protein synthesis. *Eur. J. Biochem.*, **99**, 623–628.

29. Park,W.K.C., Auer,M., Jaksche,H. and Wong,C.H. (1996) Rapid combinatorial synthesis of aminoglycoside antibiotic mimetics: use of a polyethylene glycol-linked amine and a neamine-derived aldehyde in multiple component condensation as a strategy for the discovery of new inhibitors of the HIV RNA rev responsive element. *J. Am. Chem. Soc.*, **118**, 10150–10155.

30. Bernacchi,S., Ennifar,E., Toth,K., Walter,P., Langowski,J. and Dumas,P. (2005) Mechanism of hairpin-duplex conversion for the HIV-1 dimerization initiation site. *J. Biol. Chem.*, **280**, 40112–40121.

31. Vicens,Q. and Westhof,E. (2001) Crystal structure of paromomycin docked into the eubacterial ribosomal decoding A site. *Structure Fold Des.*, **9**, 647–658.

32. Jones,T.A. (1978) A graphic model building and refinement system for macromolecules. *J. Appl. Crystallogr.*, **11**, 268–272.

33. Brunger,A.T., Adams,P.D., Clore,G.M., DeLano,W.L., Gros,P., Grosse-Kunstleve,R.W., Jiang,J.S., Kuszewski,J., Nilges,M. *et al.* (1998) Crystallography & NMR system: a new software suite for macromolecular structure determination. *Acta Crystallogr. D. Biol. Crystallogr.*, **54**, 905–921.

34. Velazquez Campoy,A. and Freire,E. (2005) ITC in the post-genomic era...? Priceless. *Biophys. Chem.*, **115**, 115–124.

35. Kaul,M., Barbieri,C.M., Kerrigan,J.E. and Pilch,D.S. (2003) Coupling of drug protonation to the specific binding of aminoglycosides to the A site of 16 S rRNA: elucidation of the number of drug amino groups involved and their identities. *J. Mol. Biol.*, **326**, 1373–1387.

36. Fukada,H. and Takahashi,K. (1998) Enthalpy and heat capacity changes for the proton dissociation of various buffer components in 0.1 M potassium chloride. *Proteins*, **33**, 159–166.

37. Kaul,M. and Pilch,D.S. (2002) Thermodynamics of aminoglycoside-rRNA recognition: the binding of neomycin-class aminoglycosides to the A site of 16S rRNA. *Biochemistry*, **41**, 7695–7706.

38. Tam,V.K., Kwong,D. and Tor,Y. (2007) Fluorescent HIV-1 dimerization initiation site: design, properties, and use for ligand discovery. *J. Am. Chem. Soc.*, **129**, 3257–3266.

39. Han,Q., Zhao,Q., Fish,S., Simonsen,K.B., Vourloumis,D., Froelich,J.M., Wall,D. and Hermann,T. (2005) Molecular recognition by glycoside pseudo base pairs and triples in an apramycin-RNA complex. *Angew. Chem. Int. Ed. Engl.*, **44**, 2694–2700.

40. Brodersen,D.E., Clemons,W.M.Jr, Carter,A.P., Morgan-Warren,R.J., Wimberly,B.T. and Ramakrishnan,V. (2000) The structural basis for the action of the antibiotics tetracycline, pactamycin, and hygromycin B on the 30S ribosomal subunit. *Cell*, **103**, 1143–1154.

41. Kaul,M., Barbieri,C.M. and Pilch,D.S. (2005) Defining the basis for the specificity of aminoglycoside-rRNA recognition: a comparative study of drug binding to the A sites of Escherichia coli and human rRNA. *J. Mol. Biol.*, **346**, 119–134.

42. Kaul,M., Barbieri,C.M. and Pilch,D.S. (2006) Aminoglycoside-induced reduction in nucleotide mobility at the ribosomal RNA A-site as a potentially key determinant of antibacterial activity. *J. Am. Chem. Soc.*, **128**, 1261–1271.

43. Pilch,D.S., Kaul,M., Barbieri,C.M. and Kerrigan,J.E. (2003) Thermodynamics of aminoglycoside-rRNA recognition. *Biopolymers*, **70**, 58–79.

44. Wong,C.H., Hendrix,M., Priestley,E.S. and Greenberg,W.A. (1998) Specificity of aminoglycoside antibiotics for the A-site of the decoding region of ribosomal RNA. *Chem. Biol.*, **5**, 397–406.

45. Shandrick,S., Zhao,Q., Han,Q., Ayida,B.K., Takahashi,M., Winters,G.C., Simonsen,K.B., Vourloumis,D. and Hermann,T. (2004) Monitoring molecular recognition of the ribosomal decoding site. *Angew. Chem. Int. Ed. Engl.*, **43**, 3177–3182.

46. Alper,P.B., Hendrix,M., Sears,P. and Wong,C.-H. (1998) Probing the specificity of aminoglycoside-ribosomal RNA interactions with designed synthetic analogs. *J. Am. Chem. Soc.*, **120**, 1965–1978.

47. Ma,C., Baker,N.A., Joseph,S. and McCammon,J.A. (2002) Binding of aminoglycoside antibiotics to the small ribosomal subunit: a continuum electrostatics investigation. *J. Am. Chem. Soc.*, **124**, 1438–1442.

48. Puglisi,J.D. and Tinoco,I.Jr. (1989) Absorbance melting curves of RNA. *Methods Enzymol.*, **180**, 304–325.

49. Laughrea,M. and Jetté,L. (1996) Kissing-loop model of HIV-1 genome dimerization: HIV-1 RNA can assume alternative dimeric forms, and all sequences upstream or downstream of hairpin 248-271 are dispensable for dimer formation. *Biochemistry*, **35**, 1589–1598.

50. Muriaux,D., Fossé,P. and Paoletti,J. (1996) A kissing complex together with a stable dimer is involved in the HIV-1_Lai RNA dimerization process *in vitro*. *Biochemistry*, **35**, 5075–5082.

51. Baba,S., Takahashi,K., Nomura,Y., Noguchi,S., Koyanagi,Y., Yamamoto,N., Takaku,H. and Kawai,G. (2001) Conformational change of dimerization initiation site of HIV-1 genomic RNA by NCp7 or heat treatment. *Nucleic Acids Res. Suppl.*, **1**, 155–156.

52. Theilleux-Delalande,V., Girard,F., Huynh-Dinh,T., Lancelot,G. and Paoletti,J. (2000) The HIV-1(Lai) RNA dimerization. Thermodynamic parameters associated with the transition from the kissing complex to the extended dimer. *Eur. J. Biochem.*, **267**, 2711–2719.

53. Chworos,A., Severcan,I., Koyfman,A.Y., Weinkam,P., Oroudjev,E., Hansma,H.G. and Jaeger,L. (2004) Building programmable jigsaw puzzles with RNA. *Science*, **306**, 2068–2072.

54. Hansma,H.G., Oroudjev,E., Baudrey,S. and Jaeger,L. (2003) TectoRNA and 'kissing-loop' RNA: atomic force microscopy of self-assembling RNA structures. *J. Microsc.*, **212**, 273–279.

55. Horiya,S., Li,X., Kawai,G., Saito,R., Katoh,A., Kobayashi,K. and Harada,K. (2003) RNA LEGO: magnesium-dependent formation of specific RNA assemblies through kissing interactions. *Chem. Biol.*, **10**, 645–654.